INTERNATIONAL ATOMIC ENERGY AGENCY
UNITED NATIONS EDUCATIONAL, SCIENTIFIC AND CULTURAL ORGANIZATION

INTERNATIONAL CENTRE FOR THEORETICAL PHYSICS
34100 TRIESTE (ITALY) - P.O.B. 586 - MIRAMARE - STRADA COSTIERA 11 - TELEPHONES: 224281/2/3/4/5/6
CABLE: CENTRATOM - TELEX 460392-1

SMR/98 - 35

AUTUMN COURSE ON GEOMAGNETISM, THE IONOSPHERE AND MAGNETOSPHERE

(21 September - 12 November 1982)

# DIRECTION OF ENERGY PROPAGATION FOR ELF-VLF WAVES IN A HOMOGENEOUS MAGNETOPLASMA

M. DOBROWOLNY
Istituto Fisica Spazio Interplanetario
C.N.R.
C.P. 27
00044 Frascati (Roma)
ITALY

# 4. DIRECTION OF ENERGY PROPAGATION FOR ELF-VLF WAVES IN A HOMOGENEOUS MAGNETOPLASMA

## 4.1 Introduction

As the first step in investigating guidance of electromagnetic waves in the ionosphere and magnetosphere along magnetic field lines, we will consider in this section the direction of wave group velocity with respect to the static magnetic field. We will do that for ELF and VLF waves and referring, for the time being, to a homogeneous magnetoplasma (and, hence, not the real ionospheric and magnetospheric media).

The angle $\psi$ between group velocity and magnetic field direction is

$$\psi = \theta - \alpha \tag{4.1}$$

with $\theta$ the wave angle with respect to $\underline{H}_o$ and $\alpha$ the angle between wave normal and group velocity derived in Sect. 3

$$tg\alpha = \frac{1}{n}\frac{\partial n}{\partial \theta} \tag{4.2}$$

An explicit formula for $\psi$, in terms of the refractive index is

$$tg\psi = \frac{\partial(n\cos\theta)/\partial\cos\theta}{\partial(n\cos\theta)/\partial\cos\theta - \frac{1}{\cos\theta}\partial n/\partial\cos\theta} \tag{4.3}$$

In the following Sections we will first give approximate analytical results for the angle $\psi$, for VLF and ELF waves and then show more general results from numerical calculations. These will give us a first idea on guidance of VLF and ELF waves along the magnetic field.



## 4.2 Whistler rays

In Sect. 3 we have derived for whistler waves at frequencies

$$\omega < \omega_{Be} \tag{4.4}$$

the approximate results for the refractive index, valid for Quasi-Longitudinal (QL) propagation

$$n^2 = \frac{B^2}{\Lambda(\cos\theta - \Lambda)} \tag{4.5}$$

where we have introduced now the normalized frequency

$$\Lambda = \frac{\omega}{|\omega_{Be}|} \tag{4.6}$$

and

$$B = \frac{\omega_{pe}}{|\omega_{Be}|} \tag{4.7}$$

Corresponding to (4.5) we have for the wave frequency,

$$\omega(K,\theta) = \frac{|\omega_{Be}|K^2c^2\cos\theta}{\omega_{pe}^2 + K^2c^2} \tag{4.8}$$

We will now show, following the early work of Storey (1953) that some fundamental properties of the whistler phenomenon namely, the tendency of whistlers to follow magnetic field lines and the characte-

ristic shape of a whistler sonogram (i.e. a frequency versus time diagram), can be shown to be simple consequences of the above formulae.

First of all, from (4.5) we can draw, for any given value of the frequency, the refractive index surface of whistler waves. The typical shapes that one obtains are shown in Fig. 18 where the three curves refer to the cases: $\Lambda \sim 0$ (curve (a)), $0<\Lambda<0.5$ (curve (b)), $0.5<\Lambda<1$ (curve (c)). The normals to the various points of the curve of refractive index give, as we saw in Sect. 3, the ray direction. Thus we see clearly, for example on curve (a) referring to low frequencies, the tendency for whistler rays to bend towards the direction of the static magnetic field. There we see that, for very large wave normal angles, the ray would come back and approach the direction of the magnetic field. When the wave normal angle reaches 90° we have the curious physical picture of a wave packet with its wave crests going in one direction (the direction of the wave normal) while the wave packet itself moves off in a perpendicular direction.

To see this more quantitatively we use the index of refraction (4.5) in (4.2), (4.3) thus obtaining

$$tg\alpha = \frac{\sin\theta}{2(\cos\theta - \Lambda)} \qquad (4.9)$$

$$tg\psi = \frac{\sin\theta\,(\cos\theta - 2\Lambda)}{1 + \cos\theta\,(\cos\theta - 2\Lambda)} \qquad (4.10)$$

Fig.19a (from Helliwell, 1965) gives the corresponding behaviour of the angle of the ray with respect to the magnetic field as a function of $\theta$, for various values of $\Lambda$. The curve corresponding to $\Lambda=0$ has its maximum $\psi_{max}$ at $\theta=54°$ and $\psi_{max}=19°29'$. This is the famous Storey's limiting angle for whistler ray propagation at very low frequencies



$\Lambda<<1$, the meaning being that, at this low frequency limit of the whistler's spectrum, rays do not depart more than $\sim 20°$ from the magnetic field direction. In general with respect to frequency, the maximum positive value of $\psi$ is obtained by equating to 0 the derivative of (4.10) with respect to $\theta$. The result is (Helliwell, 1965)

$$tg\,\psi_H^{pos} = \frac{\left[\left(1-\Lambda^2\right)^{1/2} - \sqrt{3}\,\Lambda\right]^{3/2}}{2^{3/2}\left(1-\Lambda^2\right)^{3/4}} \qquad (4.11)$$

The maximum negative value of $\psi$ is, on the other hand, determined by the condition $\cos\theta=\Lambda$ which defines (see eq. (4.5)) the maximum possible value of $\theta$ for wave propagation. Using this limit in (4.10) we obtain

$$tg\,\psi_H^{neg} = \theta - \frac{\pi}{2} \qquad (4.12)$$

which is the straight line drawn in the negative $\psi$ region of Fig. 19a. Equations (4.11) and (4.12) together express the limits of ray direction for which QL propagation of whistler is possible a homogeneous magnetoplasma. These are drawn in Fig.19b (always taken from Helliwell, 1965) where the higher of the two values is drawn solid to indicate the maximum possible ray direction regardless of sign. The minimum ray cone is of $\sim 11°$ and occurs at $\Lambda=0.189$. Again, $\Lambda=0$ gives the value 19°20' of Storey for the ray cone. The angle of the ray with respect to the magnetic field increases with $\Lambda$ and $\psi=90°$ for $\Lambda=1$ so that we can say that, upon approaching the electron cyclotron frequency, the tendency of the waves to be guided by magnetic field lines is lost. Typical whistlers however correspond to normalized frequencies $\Lambda$ below $\sim 0.6$ and this value corresponds to an half ray cone of $\sim 37°$. To this extent therefore we may talk of guiding of whistler along magnetic field lines.

It should be taken into account that the guiding we have been talking about, besides referring to a homogeneous magnetoplasma, is only a result of the anisotropy of the medium. For the real ionosphere and magnetosphere, these preliminary conclusions on guiding will actually not be valid and, in order to explain the observed guidance properties of whistlers, we will have to introduce another form of guiding, so called geomagnetic ducting, related to the presence of field aligned density irregularities in the ionosphere.

## 4.3 Whistler's group delay

Having derived some feeling for whistler's guiding along magnetic field lines, let us now derive, from the dispersion law (4.5), the impulse response (expected for example at the ground) for a whistler propagating along a given path. As we will see, this will reproduce the characteristic descending audio tone of whistler's signals.

From (4.5) we can derive the absolute value of the group velocity

$$V_G = 2c\,\Lambda^{1/2}\left(\cos\theta - \Lambda\right)^{3/2}\frac{1}{B\cos\theta} \qquad (4.13)$$

When $\Lambda \ll \cos\theta$, this gives the approximate group velocity expression used in the early work of Eckersley and Storey on whistlers, i.e.

$$V_G = \frac{2c}{B}\left(\Lambda\cos\theta\right)^{1/2} \qquad (4.14)$$

From these expressions one can derive the delay time of a whistler signal travelling along a given path. Based on the fact that, as we have seen, the ray direction tends to be pressed to the magnetic field direction, one can assume, in a first instance, that the ray trajectory



coincides with a magnetic line of force (this is what was done in the early work on the subject). Then the group delay is simply found from

$$T = \int_{path}\frac{ds}{V_G} \qquad (4.15)$$

and, using (4.13),

$$T = \frac{\ell}{c}B\,\frac{1}{2\Lambda^{1/2}\left(1-\Lambda\right)^{3/2}} \qquad (4.16)$$

$\ell$ being the length of the magnetic line between two conjugate points of the Earth. The corresponding time $\hat{T}$, normalized to $\ell = c/B$ and hence given by

$$\hat{T} = \frac{1}{2\Lambda^{1/2}\left(1-\Lambda\right)^{3/2}} \qquad (4.17)$$

is plotted, versus $\Lambda$, in Fig. 20 which, as we see immediately, resembles closely the frequency versus time diagrams of the whistler's recording.

In a homogeneous medium T has a minimum at the frequency

$$\omega_N = \frac{|\omega_{Be}|}{4} \qquad (4.18)$$

which is called the nose frequency of the whistler. When $\Lambda \ll 1$, it is $T \sim 1/2\Lambda^{1/2}$ and there is no nose in the diagram. Clearly this approximation is then valid only much below the actual nose frequency of the whistler. In the simple homogeneous model to which Fig. 20 refers, the nose frequency does not depend from the electron plasma frequency. In a more realistic model with a non homogeneous ionosphere and magnetosphere (with both $\omega_{pe}$ and $\omega_{Be}$ functions of the path), things are more

complicated and one gets some other value for the nose frequency. For the standard model with the ionization in diffusive equilibrium one obtains (Helliwell, 1970).

$$\omega_N = 0.42 \left|\omega_{Be}^{(o)}\right| \qquad (4.19)$$

$\omega_{Be}^{(o)}$ being the minimum value of the gyrofrequency along the path.

This clearly indicates the utility of whistlers data to study ionization along the path. In particular, the expression (4.13) for the group velocity indicates that $V_G$ is small especially near the top of the path so that much of the time delay, recorded for example at the ground, will be produced near the top of the path. As the frequency versus time curve (and, in particular, the nose frequency) depends from the distribution of ionization along the path, it becomes then possible to obtain from these data good estimates of the distribution at the top of the whistler's path (for example in the magnetosphere) if one makes reasonable estimates about the shape of the distribution along a given magnetic field line.

For the use of whistler's observations to infer magnetospheric properties, the reader is adressed to the review paper of Brice and Smith (1971).

## 4.4 ELF rays

Referring to frequencies

$$\omega \ll \omega_{Bi} \qquad (4.20)$$

the expressions for the refractive indices of the A and the FMS branches are given respectively by (see Sect. 2)



$$n_-^2 = \frac{n_A^2}{\cos^2\theta} \qquad (4.21)$$

$$n_+^2 = n_A^2 \equiv \frac{c^2}{V_A^2} \qquad (4.22)$$

Using (4.2) and (4.21) we derive, for the A wave

$$\operatorname{tg}\alpha = \operatorname{tg}\theta \qquad (4.23)$$

so that $\psi=0$ and, for very low frequencies, as it is well known, the Alfvén wave energy is exactly channelled along the magnetic field, the group velocity being equal to the Alfvén speed

$$V_G = V_A$$

Upon approaching the ion cyclotron frequency, we must use for the refractive index of the same A branch (which then becomes the ion cyclotron wave)

$$n_-^2 \sim n_A^2 \frac{\omega_{Bi}^2}{\omega_{Bi}^2 - \omega^2} \frac{1+\cos^2\theta}{\cos^2\theta} \qquad (4.24)$$

Then, again from (4.2), we obtain

$$\operatorname{tg}\alpha = \frac{\operatorname{tg}\theta}{1+\cos^2\theta} \qquad (4.25)$$

and, consequently,

$$\operatorname{tg}\psi = \operatorname{tg}\theta \frac{\cos^2\theta}{1+\cos^4\theta} \qquad (4.26)$$

From this it is easily found that the maximum angle $\psi_M$ between ray direction and magnetic field is

$$\psi_M \sim 12^\circ,3 \tag{4.27}$$

so that ELF waves of the A branch continue to be rather well guided by the magnetic field also for frequencies approaching $\omega_{Bi}$. More precisely, as it turns out from numerical calculations (see Sect. 4.5), going downward in frequency the maximum cone angle decreases, scaling approximately as

$$\psi_M \sim \left(\frac{\omega}{\omega_{Bi}}\right)^{1/2} \tag{4.28}$$

until it becomes zero for $\omega=0$.

Going now over to the FMS branch, in the limit $\omega \ll \omega_{Bi}$, we find from (4.2) and (4.22) that

$$tg\alpha = 0 \tag{4.29}$$

i.e. the group velocity has the direction of the wave normal so that there is no guiding at all for low frequency magnetosonic waves. As we will see from numerical results to be reported in the next section, this absence of guiding for ELF waves of the FMS branch continues to be present also for higher frequencies approaching the ion cyclotron frequency.



## 4.5 Some numerical results for the direction of the group velocity of ELV-VLF waves in a multicomponent magnetoplasma

### 4.5.1 Introduction

We will now give some numerical results (Al'pert, 1980) for the angle $\alpha(\omega,\theta)$ with respect to the magnetic field of the group velocity of waves of frequencies $\omega<\omega_{Be}$. In the case of a plasma with only one ion component these results contain what was already derived in the previous sections with the use of approximate analytical formulas and, in addition, cover frequency ranges which were not included by the previous approximations. Results will also be given for a magnetoplasma with more than one ion component, as it is more realistic for the ionospheric plasma up to 1000-1500 km of altitude. These will give information on guiding of the new branches of waves which arise as a consequence of having multiple ion components.

All the results follow from numerical calculations from the following general formula for the angle $\alpha(\omega,\theta)$ (Al'pert, 1980)

$$tg\alpha = tg\theta\left[\epsilon_2^2 n_\pm^2 \cos^2\theta + \frac{\epsilon_1^2}{\epsilon_3}\left(n_\pm^2 - \frac{\epsilon_1^2-\epsilon_2^2}{\epsilon_1}\right)\right] \cdot \left[\epsilon_2^2 n_\pm^2 \cos^2\theta + \epsilon_1\left(n_\pm^2-\epsilon_1\right)\left(n_\pm^2 - \frac{\epsilon_1^2-\epsilon_2^2}{\epsilon_1}\right)\right]^{-1} \tag{4.30}$$

where $n_\pm$ are the solutions for the refractive index given in general by (1.10) and $\epsilon_1$, $\epsilon_2$, $\epsilon_3$ the elements of the dielectric tensor defined in Sect. 1.1.

### 4.5.2 Results for a two component plasma

Fig. 21 gives a plot of $\alpha$ versus $\theta$ (analogous to the one of Fig. 19a for whistler waves) referring to the ULF ELF regime

$$0 < \omega < \omega_{Bi}$$

and to the L wave (the Alfvén branch). The calculations refer to a ratio $\omega_{pe}/|\omega_{Be}|=2$ and to hydrogen ions. The various curves are parametrized by the values of the ratio $\omega/\omega_{Bi}$. The straight line on the right hand part of the diagram separates the regions of propagation from that of evanescence. We see here what we have already derived from approximate formulae in Sect. 4.4, namely that: 1) the waves at very low frequency ($\omega<<\omega_{Bi}$) are extremely well guided by the magnetic field; 2) good guiding is maintained also at frequencies quite close to the ion cyclotron frequency. At $\omega=0.994\ \omega_{Bi}$ the maximum of $\alpha$ is $\alpha_m \sim 12°$. Going downward in frequency we see from Fig. 21 that the maxima of the curves decrease and, as already mentioned, one finds that they scale as $(\omega/\omega_{Bi})^{1/2}$. All this shows that, indeed, the energy flux of nearly the whole branch of the A wave is very well guided by the magnetic field. However, the numerical results indicate also that, starting at a certain value of $\omega<\omega_{Bi}$ (but very close to $\omega_{Bi}$), the curve maximum of $\alpha$ vanishes (see the curve $\omega/\omega_{Bi}=0.999$ in Fig. 21) and, when $\omega \to \omega_{Bi}$, $\alpha \to -\pi/2$. It should be taken into account however that, in the immediate vicinity of $\omega_{Bi}$, cold plasma theory is certainly inappropriate.

Finally, referring always to the A branch, it is useful to look at the results on ray direction in terms of group refractive surfaces. This is illustrated in Fig. 22 (taken from Booker, 1975) where the succession of diagrams from top to bottom corresponds to decreasing frequency, from $\omega=0.8\ \omega_{Bi}$ in the upper panel to $\omega=0.01\ \omega_{Bi}$ in the lower. The horizontal arrow $\underline{B}_o$ denotes the direction of the imposed magnetic field while the other arrows indicate direction of wave propagation. It is seen that, as the frequency increases to the edge of the passband at the ion gyrofrequency, the group velocity tends to zero. On the other hand, as the frequency tends to zero, the triangular pulse pattern shrinks to a point that moves along the direction of $\underline{B}_o$ with the Alfvén velocity. An important interpretation of this figure is obtained where one considers that a point source, denoted with S in Fig. 22, is placed in the magnetoplasma, polarized as to generate only the A branch at frequencies $\omega<\omega_{Bi}$. Then we see from the figure that we can say that a magnetoplasma converts the point source (with Alfvén polarization) into a pair of end fire antennas that point in the two opposite directions $\pm\underline{B}_o$.



Passing now to the FMS branch (R wave), Fig. 23 gives the variation of $\alpha$ with $\theta$ for all the frequency regime

$$0 < \omega < \omega_{Be}$$

The solid line curves, labelled with the values of $\omega/\omega_{Be}$ down to $\omega/\omega_{Be}=0.1$, include the region of classical whistlers ($\omega_{Bi}<<\omega<<\omega_{Be}$), where ion motions do not enter dispersion relation and which we have already discussed by means of approximate formulae in Sect. 4.2. The maximum whistler's ray cone is found to be $\alpha_m \sim 19{,}5°$ close to the valued obtained by Storey and already derived analytically. Ion motions must be taken into account starting at frequencies close to the lower hybrid frequency $\omega_L$ defined by

$$\frac{1}{\omega_L^2} = \frac{1}{\omega_{Bi}^2 + \omega_{pi}^2} + \frac{1}{\omega_{Bi}|\omega_{Be}|} \qquad (4.31)$$

and the last solid line curve in Fig. 23 corresponds to $\omega=\omega_L$ while the following dashed line curves refer to $\omega<\omega_L$. It is seen that, when $\omega<\omega_L$, the angle $\alpha(\omega,\theta)$ varies initially in a complicated way. If the frequency $\omega$ is sufficiently close to $\omega_L$, in a certain interval of values of the angle $\theta$, waves are still well guided by the magnetic field: it is $\alpha<\theta$ or $\alpha<<\theta$ with two extreme points, a maximum and a minimum. However, with an increase in $\theta$, $\alpha$ begins to grow and, in any case, $\alpha\to\pi/2$ when $\theta\to\pi/2$. For frequencies $\omega<<\omega_L$ (still $\omega>\omega_{Bi}$) the waves are propagated quasi isotropically. Below $\omega_{Bi}$ (i.e. in the range of the hydromagnetic magnetoacoustic modes) and when the frequency tends to zero, as we already know, the group velocity tends to become collinear with the wave vector $\underline{k}$. This collinearity is represents by the straight line labelled $\omega/\omega_{Be}=0$ in Fig. 23.

Finally, Fig. 24 gives the group ray surfaces for the classical whistler wave between ion and electron gyrofrequencies (based on the formula (4.5) for the refractive index) and illustrates the fact that, going from $\omega_{Bi}$ to $\omega_{Be}$, this wave (especially above $\omega=\omega_L$) exhibits noticeable guiding along the magnetic field direction. As has been found by Smith (1960), the strongest beaming occurs for $\omega/\omega_{Be}=0.19$ and the corresponding minimum value of the semi-beam angle is $\sim 11°$. Apart from other complicated features of the group surfaces, we see also from the figure that beaming is gradually lost upon approaching the electron cyclotron frequency.

### 4.5.3 Results for a multicomponent plasma

When a plasma contains more than one ion species, it has correspondingly as many new branches of oscillations as it has additional ion species. In the following I will quote results obtained by Al'pert



(1980) for a plasma with three ion species, namely $O^+$, $He^+$ and $H^+$. Parameters referring to these three species will be labelled 1,2,3 respectively. The calculations refer to the following ion concentrations

$$\frac{N_1}{N_0}=0.4\quad,\quad \frac{N_2}{N_0}=0.1\quad,\quad \frac{N_3}{N_0}=0.5$$

and to $\omega_{pe}/|\omega_{Be}|=2$. In the frequency range

$$0<\omega\lesssim\omega_{B3}\equiv\omega_{BH} \tag{4.32}$$

($\omega_{BH}$ being the highest ion gyrofrequency) there are now two cut-off frequencies $\omega_{C1}$, $\omega_{C2}$ which corresponds to $n_+^2(\omega_{C1})=0$, $n_-^2(\omega_{C2})=0$ respectively and are determined from

$$\omega_{C1}+\omega_{C2}=\left(1-\frac{N_1}{N_0}\right)\omega_{B1}+\left(1-\frac{N_2}{N_0}\right)\omega_{B2}+\left(1-\frac{N_3}{N_0}\right)\omega_{B3} \tag{4.33}$$

$$\omega_{C1}\,\omega_{C2}=\frac{N_1}{N_0}\,\omega_{B2}\omega_{B3}+\frac{N_2}{N_0}\,\omega_{B3}\omega_{B1}+\frac{N_3}{N_0}\,\omega_{B1}\omega_{B2}$$

Correspondingly, in the frequency regime (4.32), there are four continuous real branches of waves:

1) a first branch of the A (ordinary) wave for $0<\omega<\omega_{B1}$
2) a second branch of the A wave for $\omega_{C1}<\omega<\omega_{B3}$
3) a first branch of the FMS (extraordinary) wave for $0<\omega<\omega_{B2}$
4) a second branch of the FMS wave for $\omega_{C2}<\omega<\omega_{B3}$

Figures 25a and b refer to the Alfvén branches and, more precisely, figure 25a is for the frequency regime 1) and Fig. 25b for the frequen-

cy regime 2). From Fig. 25a it is seen that, for frequencies smaller than the $O^+$ cyclotron frequency (the smallest cyclotron frequency in this plasma), the curves $\alpha(\omega,\theta)$ are exactly similar to those of Fig. 21 for Alfvén waves in a two component plasma. The corresponding considerations on guiding have therefore already been given.

The behaviour of the A branch in the frequency regime 2) (see Fig. 25b) is more complicated and, in order to illustrate it, we need to introduce several new typical frequencies for the multicomponent plasma under consideration.

These are the new ion-ion hybrid frequencies which are indicated by $\omega_{L12}$ $\omega_{L23}$ and are defined through

$$\omega_{L12}^2 + \omega_{L23}^2 = \left[\omega_{p1}^2\left(\omega_{B2}^2 + \omega_{B3}^2\right) + \omega_{p2}^2\left(\omega_{B3}^2 + \omega_{B1}^2\right) + \right. \tag{4.34}$$

$$\left. + \omega_{p3}^2\left(\omega_{B1}^2 + \omega_{B2}^2\right)\right]\left[\omega_{p1}^2 + \omega_{p2}^2 + \omega_{p3}^2\right]^{-1}$$

$$\omega_{L12}^2\,\omega_{L23}^2 = \frac{\omega_{p1}^2\omega_{B2}^2\omega_{B3}^2 + \omega_{p2}^2\omega_{B3}^2\omega_{B1}^2 + \omega_{p3}^2\omega_{B1}^2\omega_{B2}^2}{\omega_{p1}^2 + \omega_{p2}^2 + \omega_{p3}^2} \tag{4.35}$$

and two cross-over frequencies denoted by $\omega_{12}$ $\omega_{23}$ and determined from

$$\omega_{12}^2 + \omega_{23}^2 = \omega_{B1}^2\left(1 - \frac{N_1}{N_0}\right) + \omega_{B2}^2\left(1 - \frac{N_2}{N_0}\right) + \omega_{B3}^2\left(1 - \frac{N_3}{N_0}\right) \tag{4.36}$$



$$\omega_{12}^2\cdot\omega_{23}^2 = \frac{N_1}{N_0}\omega_{B2}^2\omega_{B3}^2 + \frac{N_2}{N_0}\omega_{B3}^2\omega_{B1}^2 + \frac{N_3}{N_0}\omega_{B1}^2\omega_{B2}^2 \tag{4.37}$$

Corresponding to the parameters used in Al'pert's calculations, it is

$$\frac{\omega_{12}}{\omega_{B3}} = 0.224, \qquad \frac{\omega_{23}}{\omega_{B3}} = 0.713, \qquad \frac{\omega_{L23}}{\omega_{B3}} = 0.359$$

as indicated in Fig. 25b. The main points from the results of Fig. 25b are:

1) at frequencies $\omega_{L23} < \omega < 0.999\ \omega_{B3}$ the ordinary (A) wave behaves exactly as the electron whistler mode of Fig. 22 (for the two component plasma considered there). Hence it is well guided by the magnetic field, with $\alpha < \alpha_m \sim 19{,}5°$. In particular, very good guidance is obtained near the cross over frequency $\omega_{23}$ (it is $\omega_{L23} < \omega_{23} < \omega_{B3}$). Guiding becomes clearly worst for $\omega < \omega_{L23}$ and disappears completely at $\omega = \omega_{12} (< \omega_{C1})$ where wave group velocity and $\underline{k}$ are collinear.

Going now to the FMS branch in the frequency regime 3), $0 < \omega < \omega_{B2}$) (see Fig. 26a) we must repeat considerations anologous to those for the A branch (between $\omega_{C1}$ and $\omega_{B3}$). Also this branch reproduces essentially the behaviour of the electron whistler wave for frequencies

$$\omega_{L12} < \omega < 0.999\ \omega_{B2}$$

and it is therefore well guided by the magnetic field. In particular, extremely good guiding is obtained also for this branch near the appropriate cross over frequency which is now $\omega_{12}$. At frequencies lower than the ion-ion hybrid frequency $\omega_{L12}$ guiding becomes worst and it is lost completely as $\omega \to 0$.

The second FMS branch, in regime 4) (see Fig. 26b) has essentially no guiding properties. In particular, at the cross over frequency $\omega_{23}$ ($\omega_{C2}<\omega_{23}<\omega_{B3}$) the group velocity and $\underline{k}$ are essentially collinear.

These results can perhaps be better visualized with reference to Fig. 27 (always taken from the work of Al'pert, 1980), which gives curves $\alpha(\omega)$ for two values of the angle $\theta$ of propagation with respect to the magnetic field, $\theta=30°$ and $\theta=50°$. The horizontal axis has indicated the positions of several of the frequencies which have been introduced and defined previously. The solid curves refer to the ordinary (A) wave branch and the dashed line curves to the extraordinary (FMS) mode. With the help of these figures we can summarize the above results in the following way: when several sort of ions exist in the plasma the ion-ion hybrid frequencies (which fall now in the ULF range) play the same role as the lower hybrid frequency $\omega_L$ of the electron whistler mode in the VLF range. For example, for the case considered of 3 ion species, for $\omega_{L23}<\omega<\omega_{B3}$, where $\omega_{L23}$ is the highest of the two ion-ion hybrid frequencies and $\omega_{B3}$ the highest of the ion cyclotron frequencies, the A branch is well guided by the magnetic field (in the same sense as ordinary whistler waves). In particular exact guiding for this branch is obtained at the highest $\omega_{23}$ of the two cross over frequencies. On the other hand, the FMS branch is also well guided (as ordinary whistlers) in the frequency range $\omega_{L12}<\omega<\omega_{B2}$, $\omega_{L12}$ being the smallest of the two hybrid frequencies and $\omega_{B3}$ the intermediate of the ion cyclotron frequencies; In particular, it is exactly guided ($\alpha=0$) at $\omega=\omega_{12}$, the smallest of the two cross-over frequencies. On the other hand, the FMS wave is not at all guided outside the above range and, in particular, becomes isotropic at $\omega=\omega_{23}$ (where the A branch is exactly guided).

Thus, in short, it can be said that the presence of more than one ion species in the plasma extends the good guiding properties of



the VLF whistlers in the ELF-ULF range (and it does so, in different frequency ranges both for the ordinary and the extraordinary mode). These well guided ULF branches are sometimes referred to as ion whistlers.

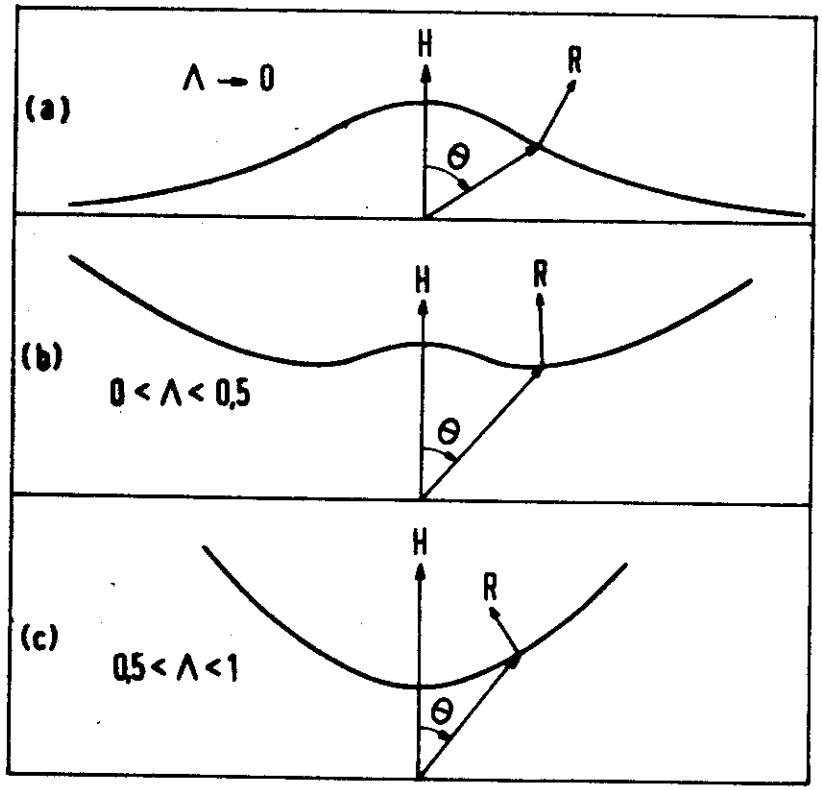
(a)
Λ → 0
H
R
Θ
(b)
0 < Λ < 0,5
H
R
Θ
(c)
0,5 < Λ < 1
H
R
Θ

FIG. 18



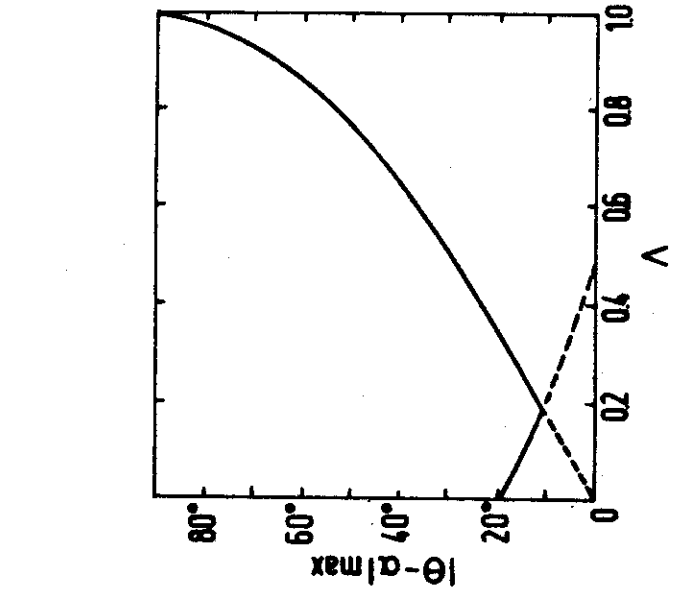
|Θ-αl|max
80°
60°
40°
20°
0
0,2
0,4
0,6
0,8
1,0
Λ

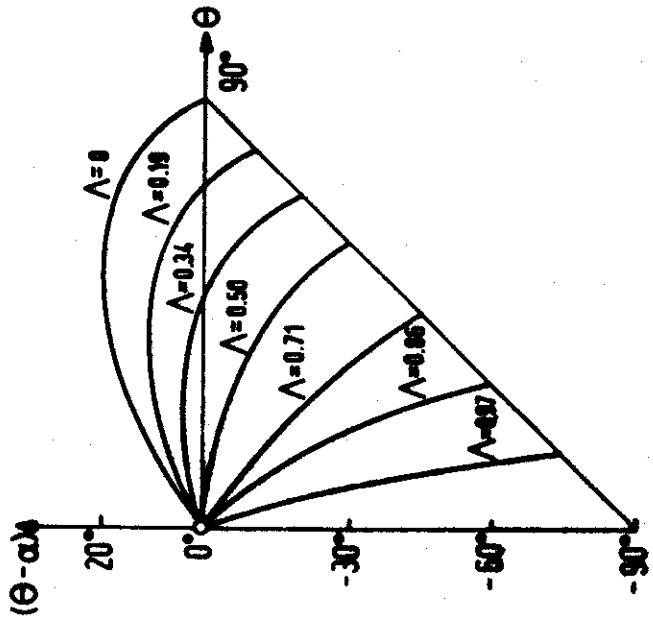
Θ
90°
Λ=0
Λ=0,18
Λ=0,34
Λ=0,50
Λ=0,71
Λ=0,85
Λ=1
(Θ-αl)
20°
0°
-30°
-60°
-90°

FIG. 19

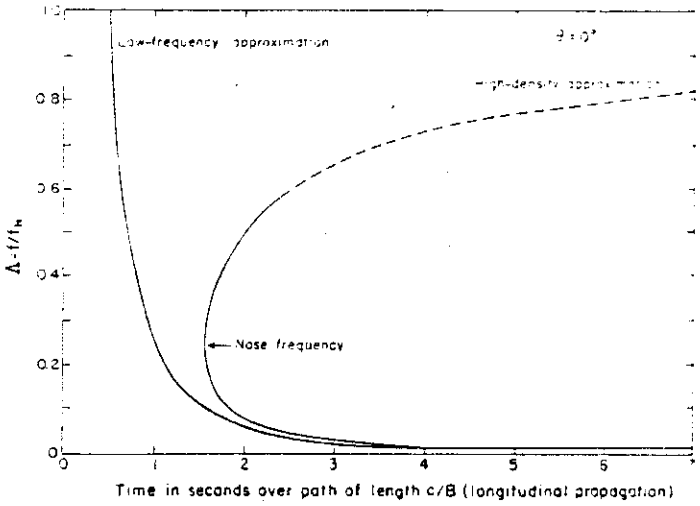
Low-frequency approximation
Nose frequency
Time in seconds over path of length c/B (longitudinal propagation)

FIG. 20



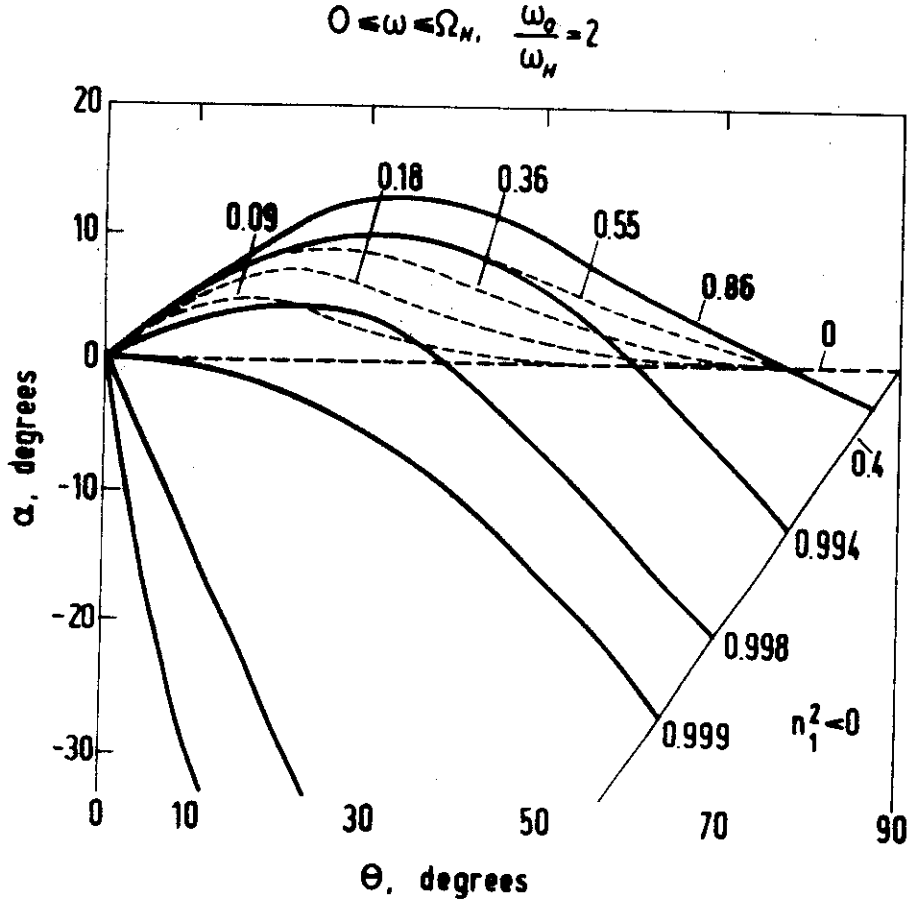
0 ≤ ω ≤ Ω_H, ω_p/ω_H = 2
0.09
0.18
0.36
0.55
0.86
0
0.4
0.994
0.998
0.999
n₁² < 0
α, degrees
θ, degrees

FIG 21

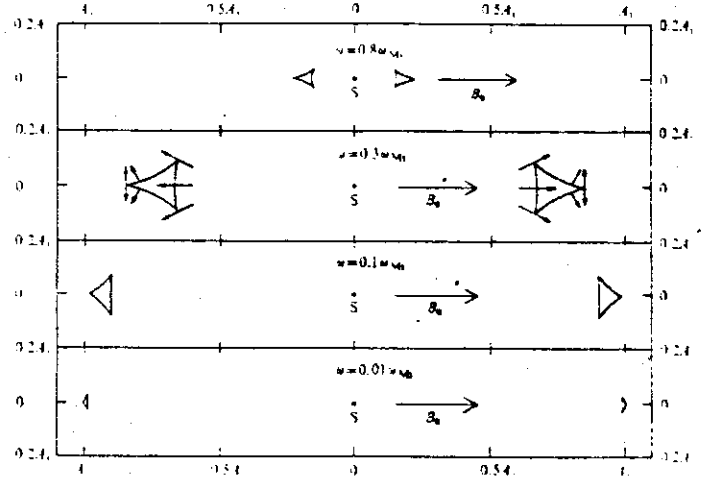

FIG 22

FIG. 23



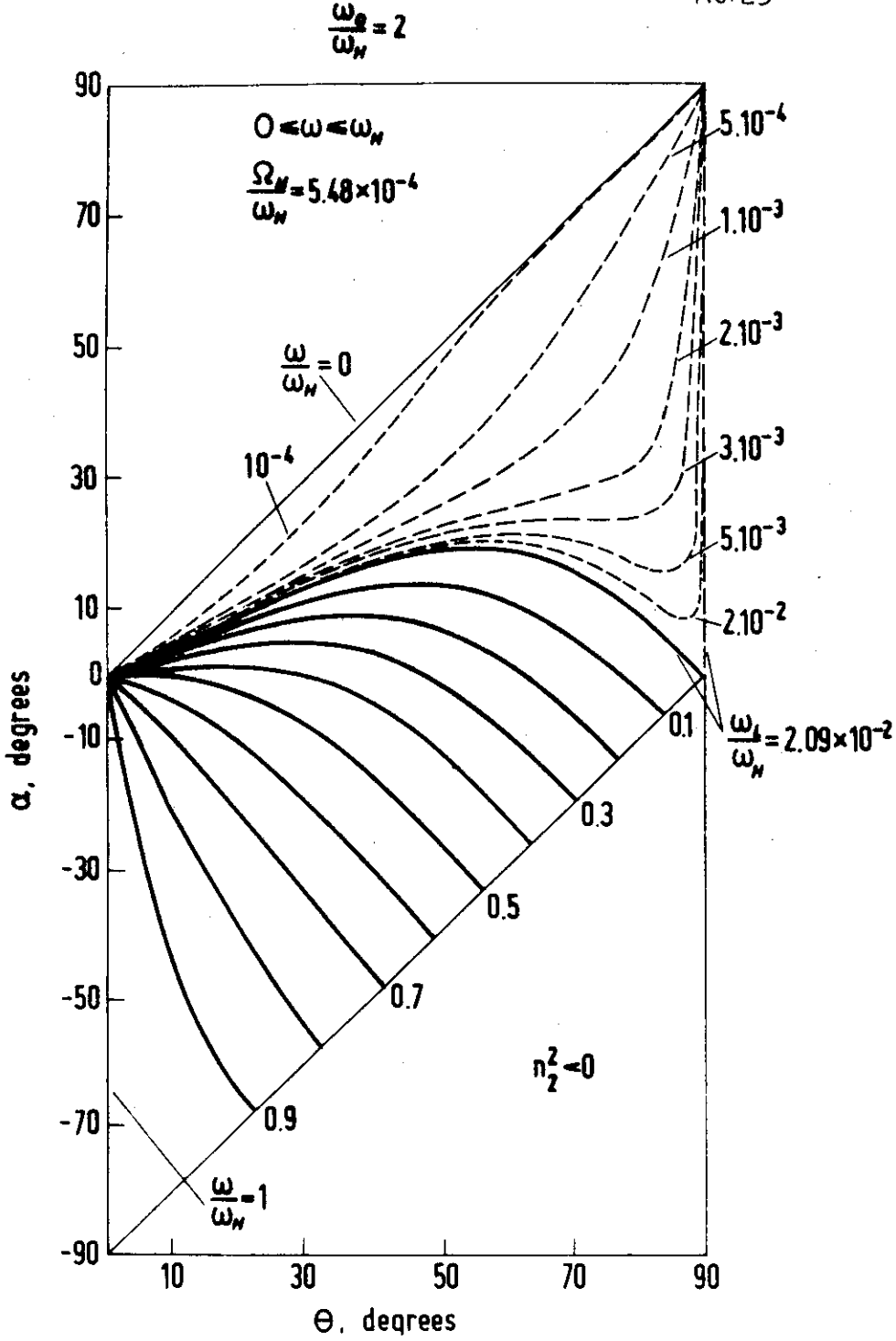
ω_e/ω_H = 2
0 ≤ ω ≤ ω_H
Ω_H/ω_H = 5.48×10⁻⁴
ω/ω_H = 0
10⁻⁴
5.10⁻⁴
1.10⁻³
2.10⁻³
3.10⁻³
5.10⁻³
2.10⁻²
ω_L/ω_H = 2.09×10⁻²
0.1
0.3
0.5
0.7
0.9
ω/ω_H = 1
n₂² < 0
α, degrees
Θ, degrees
90
70
50
30
10
0
-10
-30
-50
-70
-90
10
30
50
70
90

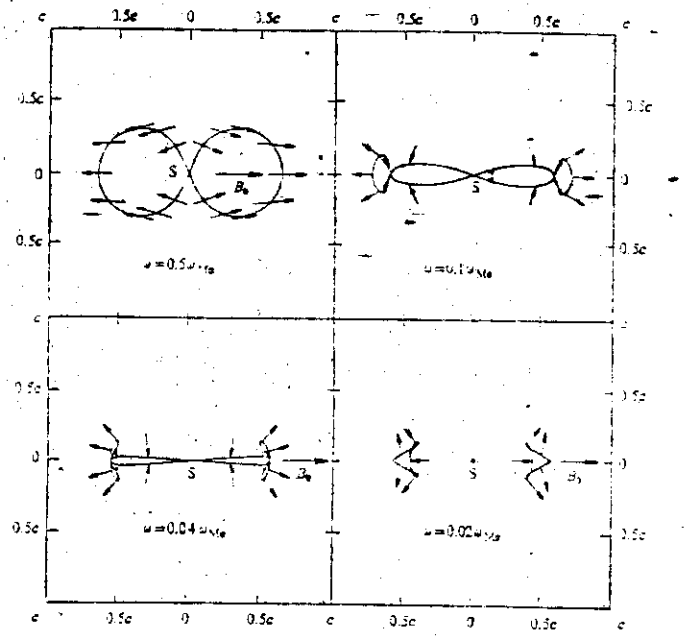

FIG. 24



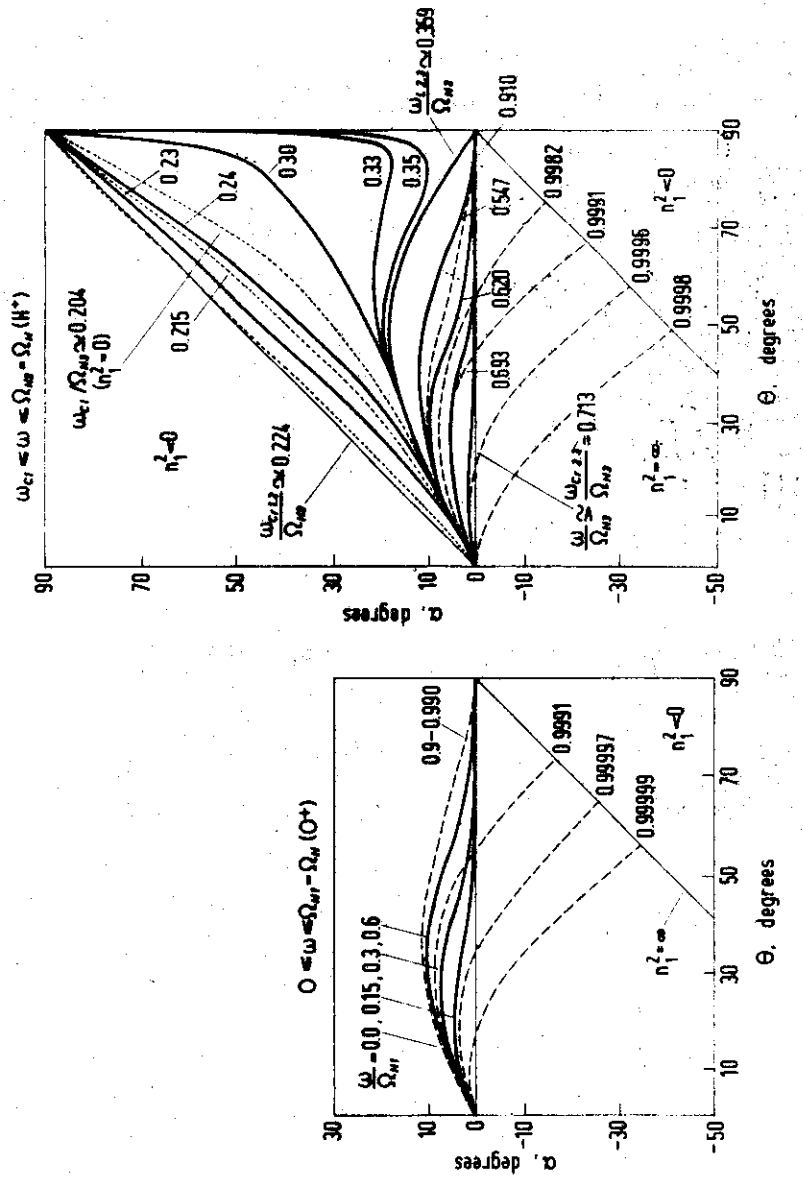
α, degrees
Θ, degrees
0.23
0.24
0.30
0.33
0.35
0.547
0.620
0.693
0.715
0.910
0.9982
0.9991
0.9996
0.9998
0.9-0.990
0.99991
0.99997
0.99999
n₁²=0
n₁²=∞

FIG. 25

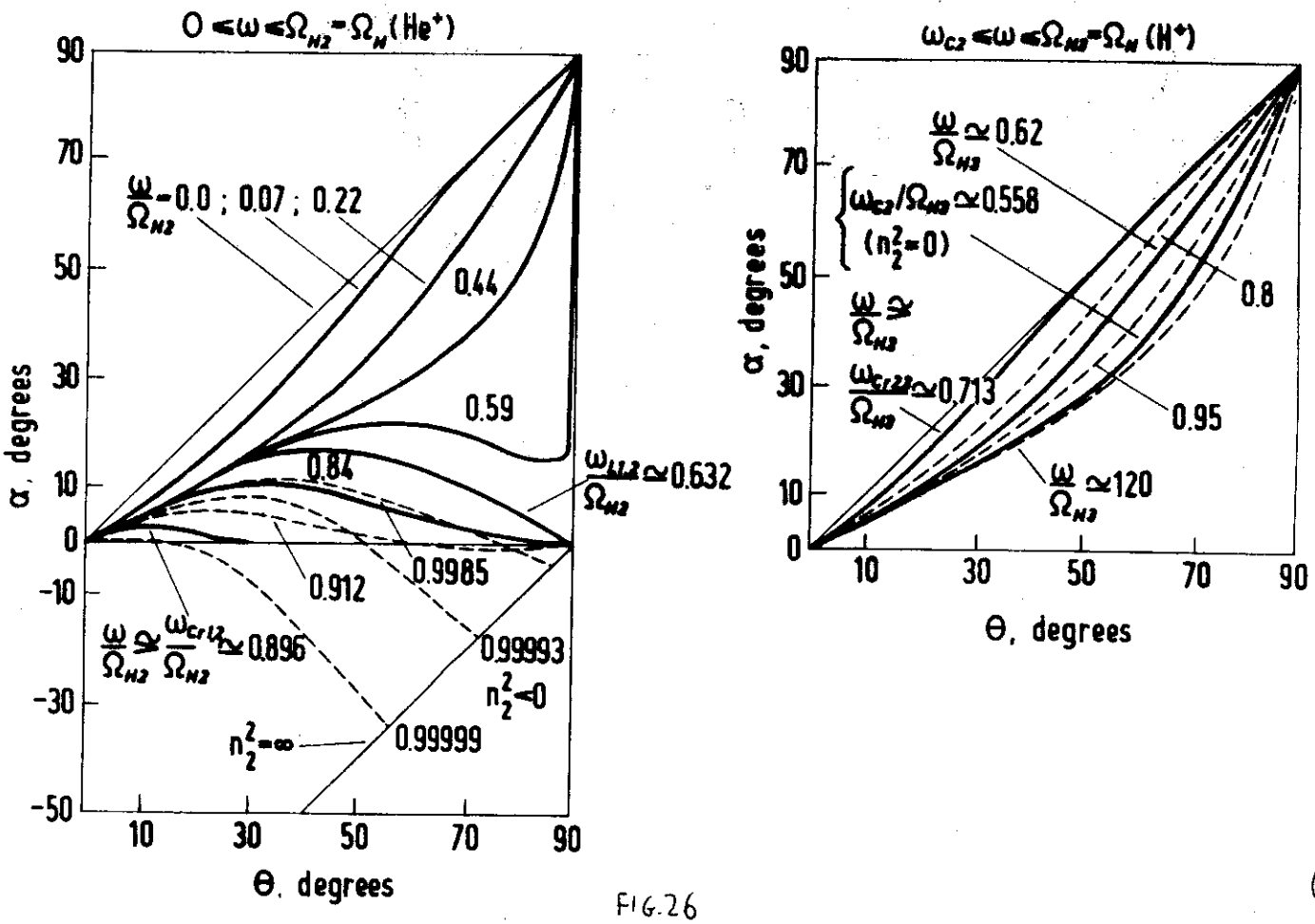
$0 \leq \omega \leq \Omega_{H2} = \Omega_H(He^+)$
$\omega_{C2} \leq \omega \leq \Omega_{H3} = \Omega_H(H^+)$
α, degrees
Θ, degrees
$\frac{\omega}{\Omega_{H2}} = 0.0 ; 0.07 ; 0.22$
0.44
0.59
0.84
$\frac{\omega_{LL2}}{\Omega_{H2}} \simeq 0.632$
0.912
0.9985
$\frac{\omega}{\Omega_{H2}} \gtrsim \frac{\omega_{Cr12}}{\Omega_{H2}} \simeq 0.896$
0.99993
$n_2^2 < 0$
$n_2^2 = \infty$
0.99999
$\frac{\omega}{\Omega_{H3}} \simeq 0.62$
$\omega_{C2}/\Omega_{H3} \simeq 0.558$
$(n_2^2 = 0)$
0.8
$\frac{\omega}{\Omega_{H3}} \gtrsim \frac{\omega_{Cr23}}{\Omega_{H3}} \simeq 0.713$
0.95
$\frac{\omega}{\Omega_{H3}} \simeq 120$

FIG.26



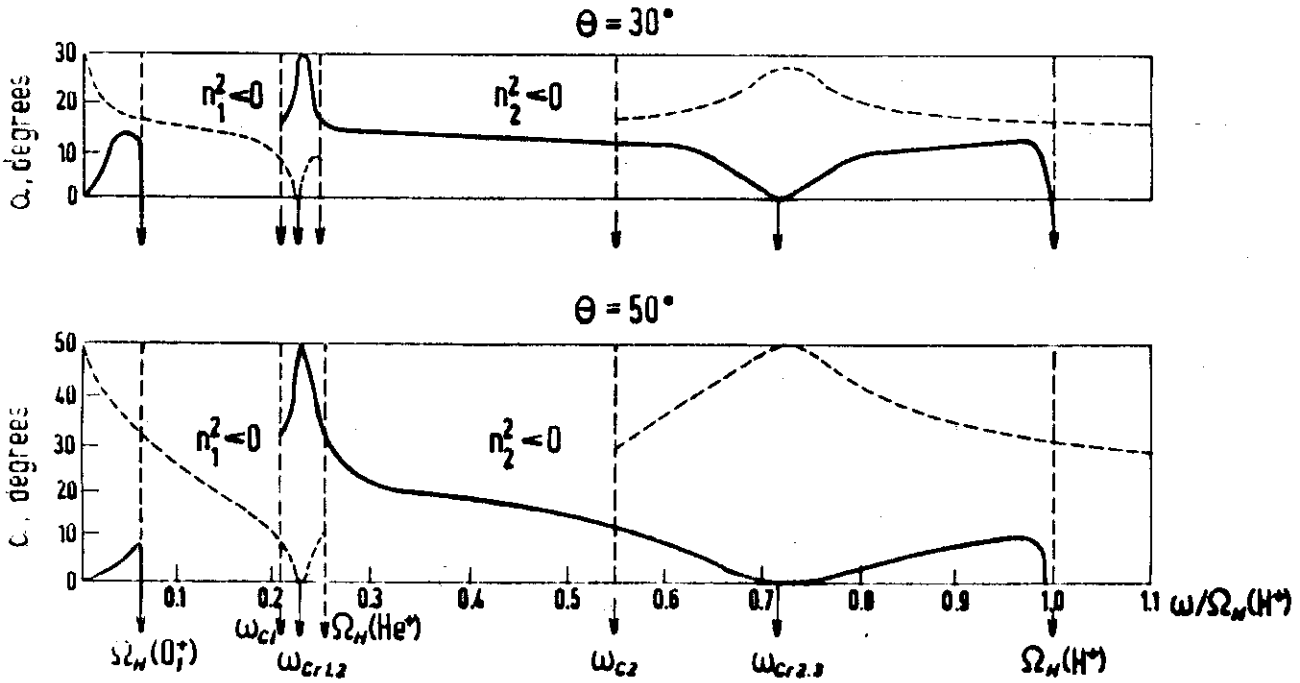
Θ = 30°
Θ = 50°
α, degrees
$n_1^2 < 0$
$n_2^2 < 0$
$\Omega_H(O_1^+)$
$\omega_{C1}$
$\omega_{Cr1,2}$
$\Omega_H(He^+)$
$\omega_{C2}$
$\omega_{Cr2,3}$
$\Omega_H(H^+)$
$\omega/\Omega_H(H^+)$

FIG.27